Synthesis and Transfer of Large-Area Monolayer WS_2 Crystals: Moving Toward the Recyclable Use of Sapphire Substrates

Zai-Quan Xu,[†,‡] Yupeng Zhang,[†] Shenghuang Lin,[†,§] Changxi Zheng,[⊥,∥] Yu Lin Zhong,[†] Xue Xia,[†] Zhipeng Li,[†] Ponraj Joice Sophia,[§] Michael S. Fuhrer,[∥] Yi-Bing Cheng,[†] and Qiaoliang Bao*[,§,†]

[†]Department of Materials Science and Engineering, Faculty of Engineering, Monash University, Clayton 3800, Victoria, Australia, [‡]The Melbourne Centre for Nanofabrication, 151 Wellington Road, Clayton 3168, Victoria, Australia, [§]Institute of Functional Nano and Soft Materials (FUNSOM), Jiangsu Key Laboratory for Carbon-Based Functional Materials and Devices, and Collaborative Innovation Center of Suzhou Nano Science and Technology, Soochow University, Suzhou 215123, P. R. China, [⊥]Department of Civil Engineering, Monash University, Clayton 3800, Victoria, Australia, and [∥]School of Physics, Monash University, Monash 3800, Victoria, Australia

ABSTRACT Two-dimensional layered transition metal dichalcogenides (TMDs) show intriguing potential for optoelectronic devices due to their exotic electronic and optical properties. Only a few efforts have been dedicated to large-area growth of TMDs. Practical applications will require improving the efficiency and reducing the cost of production, through (1) new growth methods to produce large size TMD monolayer with less-stringent conditions, and (2) nondestructive transfer techniques that enable multiple reuse of growth substrate. In this work, we report to employ atmospheric pressure chemical vapor deposition (APCVD) for the synthesis of large size (>100 μm) single crystals of atomically thin tungsten disulfide (WS_2), a member of TMD family, on sapphire substrate. More importantly, we demonstrate a polystyrene (PS) mediated delamination process *via* capillary force in water which reduces the etching time in base solution and imposes only minor damage to the sapphire substrate. The transferred WS_2 flakes are of excellent continuity and exhibit comparable electron mobility after several growth cycles on the reused sapphire substrate. Interestingly, the photoluminescence emission from WS_2 grown on the recycled sapphire is much higher than that on fresh sapphire, possibly due to *p*-type doping of monolayer WS_2 flakes by a thin layer of water intercalated at the atomic steps of the recycled sapphire substrate. The growth and transfer techniques described here are expected to be applicable to other atomically thin TMD materials.

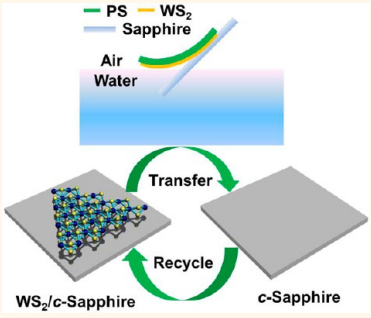

KEYWORDS: transition metal dichalcogenide · monolayer · atmospheric pressure chemical vapor deposition (APCVD) · transfer · recyclability

Atomically thin layered transition metal dichalcogenides (TMDs) of the family $(Mo,W)(S,Se)_2$ have attracted significant interest as two-dimensional semiconducting materials due to their immense potential for various applications in solar cells,[1,2] light emitting diodes,[3,4] and photosensors.[5,6] Atomically thin TMDs possess many distinctive electrical and optical properties, such as high on/off ratio,[6,7] controllable spin and valley polarization,[4] indirect band gap to direct band gap transition,[9,10] strong geometrical confinement of excitons,[11−13] and tunable photoluminescence.[14] To date, research on TMDs is largely limited by relatively small lateral size of exfoliated flakes and inefficient techniques for transfer of larger-area flakes grown by chemical vapor deposition (CVD) to substrates suitable for device fabrication. It is highly desirable to develop new techniques for the preparation and transfer of large area layered TMD crystals with high quality and continuity. Tremendous efforts have been devoted to study the growth and transfer of MoS_2;[15−24] however, there are limited reports on the preparation of large area monolayer and few-layer tungsten disulfide (WS_2).[25−27]

CVD is expected to be a promising approach to produce large area TMDs sheets for extensive device applications in view of the repeatability and controllability.

* Address correspondence to qlbao@suda.edu.cn, qiaoliang.bao@monash.edu

Received for review March 9, 2015 and accepted May 11, 2015.

Published online May 11, 2015
10.1021/acsnano.5b01480

Recently, centimeter size[25] as well as wafer scale[28] synthesis of WS_2 sheets have been demonstrated using a two-step process, which includes the pre-deposition and sulfurization of WO_3 film on SiO_2. The WS_2 sheets grown by this method are polycrystalline with the uniformity and thickness mainly inherited from the nature of pre-deposited WO_3 film, which imposes additional requirements for the deposition of atomically thin WO_3. It is noteworthy that large area, single-crystalline WS_2 monolayers with the size up to hundreds of micrometers can be successfully synthesized by sandwiching WO_3 powders in-between two pieces of SiO_2/Si substrates in CVD system.[29] The use of SiO_2 as substrate for TMDs material growth has the advantage of good compatibility for subsequent device fabrication. However, concerning the preferred nucleation at atomically flat terrace of the substrate, another hydrophilic oxide, sapphire (*i.e.*, Al_2O_3 (0001)) seems to be a more suitable substrate to grow large area, highly crystalline TMDs because the (0001) plane of *c*-sapphire is hexagonally arranged[27] matching the lattice symmetry of MoS_2, WS_2, $MoSe_2$, and WSe_2.[13,30] More recently, Zhang *et al.*[27] synthesized single crystalline WS_2 flakes with domain size up to $50 \times 50\ \mu m^2$ on *c*-sapphire substrate *via* low pressure CVD. It should be noted that the delicate control of the pressure and flow rate plays a non-negligible role in determining the morphology of WS_2 flakes. The use of atmospheric pressure chemical vapor deposition (APCVD) system to prepare layer-controllable WS_2 flakes with less-stringent growth conditions is therefore desirable. Considering the cost of the sapphire substrates, it is extremely important to develop a technique to reuse this substrate to lower the cost to prepare high quality TMDs for industrial scale applications.

In this work, we successfully demonstrate the synthesis of large area (domain size up to 135 μm), triangular monolayer WS_2 crystals on sapphire substrates *via* APCVD. More importantly, we have developed a gentle and nondestructive transfer technique which enables not only the transfer of WS_2 flakes onto arbitrary substrates without wrinkles or cracks but also the multiple reuse of sapphire substrate. Our key strategy is to use hydrophobic polystyrene (PS) as a protecting transfer layer, and to delaminate WS_2 from sapphire *via* capillary force in water. Due to the surface tension at water/air interface, WS_2-attached PS film can be peeled off in water, avoiding long time etching in hot base solution or bubble generation which could cause damage to both samples and substrates. This allows the reuse of the sapphire substrates thereby reducing the cost. In addition, the high solubility of PS in organic solvents enables quick and complete removal of the protecting layer. The growth of WS_2 with comparable lateral size on reused sapphire is demonstrated. Enhanced photoluminescence (PL) emission of WS_2 grown on recycled sapphire was observed and consistently high electron mobility was measured across three different sample growths on the same substrate. We believe that our approaches for synthesis and transfer are essential steps to improve the efficiency, reduce the production cost, and promote the current efforts of device applications.

RESULTS AND DISCUSSION

Figure 1a shows a representative optical image of monolayer WS_2 crystals on sapphire substrate synthesized by APCVD. The crystals are nearly equilateral triangular with a side length up to 135 μm, which is among the largest layered TMD crystals prepared on sapphire (0001) *via* CVD method.[25,27,31−33] Most of the crystals are monolayers, but occasionally we are able to find bilayer and trilayer regions at the center of large monolayer crystals, which is supposed to be the nucleation site.[29] It is generally believed that the growth of TMDs with CVD is a self-limiting process.[16] The lateral size of WS_2 increases with the partial pressure of chalcogen precursors,[33] and the thickness of TMD crystals could be controlled by the partial pressure of the transition metal precursors.[16] In our APCVD process, the weight of sulfur powder is ~9 times higher than WO_3, which makes the lateral growth dominating. This could be one reason for the growth of large size single crystals. Furthermore, we are able to find WS_2 single crystals with different sizes, ranging from 100 nm to 135 μm on the same sapphire substrate. The area of the crystals is proportional to the growth time before the crystal growth reaches the limit. Therefore, larger size WS_2 crystals can be expected providing the growth time is long enough.

Figure 1b shows the Raman spectra of WS_2 with different thicknesses. A predominating peak at 354 cm^{-1} is observed and assigned to the 2LA(M) mode for monolayer WS_2. The peak at 412 cm^{-1} corresponding to the A_{1g} mode, although weak, is observed as well. The separation between these two peaks is enlarged from 67 to 72 cm^{-1} with increasing thickness from monolayer to trilayer due to the red-shift of the 2LA(M) mode, consistent with previous reports.[25,31,32] Figure 1c depicts the PL spectra of monolayer, bilayer and trilayer WS_2 excited by 532 nm laser. The PL spectrum for monolayer WS_2 exhibits a strong emission peak centered at ~620 nm, corresponding to the A excitonic emission.[13,31] The PL intensity dramatically decreases as the thickness increases from monolayer to trilayer, *i.e.*, bilayer and trilayer preserve 5% and 2.5% peak intensity, respectively, of the monolayer (inset of Figure 1c). Besides, with the increase in thickness, the PL peak red-shifts (from 620 nm for monolayer, 627 nm for bilayer to 636 nm for trilayer) and the spectral width is broadened indicating the transition from direct to indirect bandgap.

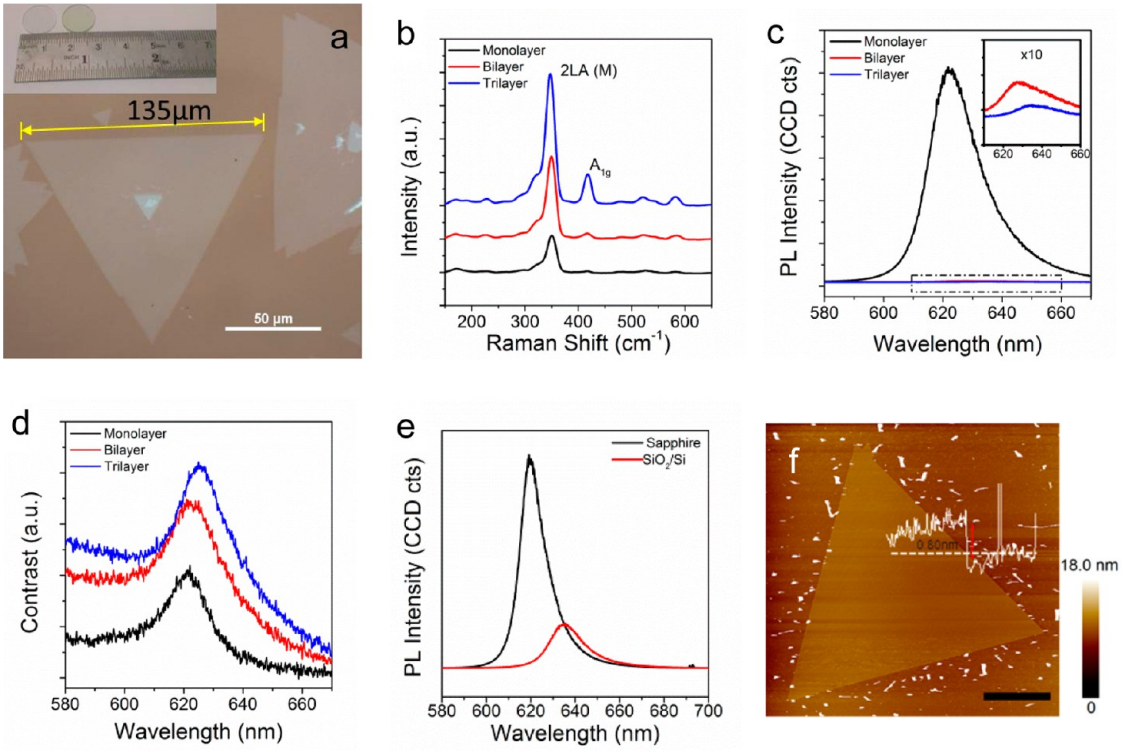

Figure 1. (a) Optical micrograph of a large WS_2 monolayer triangular flake with a side length of about 135 μm. Inset shows the photograph of WS_2 sample grown on *c*-sapphire (0001) substrate. (b and c) Raman and photoluminescence spectra for the monolayer, bilayer and trilayer WS_2 obtained with WiTec confocal Raman spectrometer excited by 532 nm laser. The inset in (c) shows the PL spectra for bilayer and triple layer WS_2 flakes. (d) Contrast spectra for the monolayer, bilayer and trilayer WS_2. (e) Comparison of PL spectra of WS_2 grown directly on sapphire and silica *via* APCVD. (f) AFM image of WS_2 monolayer crystal grown on sapphire substrate with the AFM cross-section height profile for the sample as inset. Scale bar: 8 μm.

The number of layers of WS_2 crystals are further confirmed by contrast spectroscopy, as shown in Figure 1d. The contrast is defined as

$$\text{Contrast} = \frac{I - I_b}{I_b} \quad (1)$$

where I and I_b refer to the reflected signals from WS_2 and the background, respectively. It is found that the contrast value at 630 nm has a linear relationship with the number of layers (see Supporting Information Figure S1), in good agreement with previous reports.[31,34] The contrast spectrum for monolayer WS_2 has a peak at around 620 nm, and the peak red-shifts with the increase in the number of layers, which is consistent with the observations in PL spectra.

It is noteworthy that monolayer WS_2 can also be synthesized on SiO_2/Si substrate with the same APCVD method. However, the lateral size of the WS_2 grown on SiO_2/Si is about 10 μm and the maximum size is up to 30 μm (see Figure S2), which is much smaller than those grown on sapphire. Figure 1e shows the PL spectra of WS_2 monolayers prepared on sapphire and SiO_2/Si substrates and their Raman spectra are presented in Figure S3. It is found that WS_2 on SiO_2/Si has a PL peak centered at 636 nm with a full-width at half-maximum (FWHM) of 19.8 nm. In comparison, WS_2 on sapphire has a PL peak centered at 620 nm with a FWHM of 13.3 nm. The different peak positions might have originated from different doping caused by the substrate.[35] More importantly, the PL intensity of WS_2@sapphire is about four times stronger than that of WS_2@silica. The strong emission and sharpness of the PL spectrum attest to high optical yield of our monolayer WS_2 sample grown on sapphire. The topography of monolayer WS_2 triangle grown on sapphire is investigated by the atomic force microscope (AFM), as shown in Figure 1f. The whole crystal is nearly atomically flat and clean. The height profile shows a sapphire/WS_2 step of 0.8 nm (inset) further confirming the thickness to be monolayer.

To identify the chemical composition of monolayer WS_2, X-ray photoemission spectroscopy (XPS) was used to measure the binding energy of W and S. Figure 2a,b shows the binding energy profile for W 4f and S 2p. Three peaks at 33.67, 35.86, and 38.87 eV are attributed to the W $4f_{7/2}$, W $4f_{5/2}$, and W $4f_{3/2}$, respectively. The peaks with binding energy of 162.48 and 163.60 eV can be assigned to the S $2p_{1/2}$ and S $2p_{3/2}$, respectively. All these results are consistent with the reported values for WS_2 crystal. The positions of these XPS peaks suggested that the valence of W is +4, an evidence for the formation of pure WS_2 phase.[28,36] A full range of XPS spectrum is presented in Figure S4a, in which the peaks from all the elements,

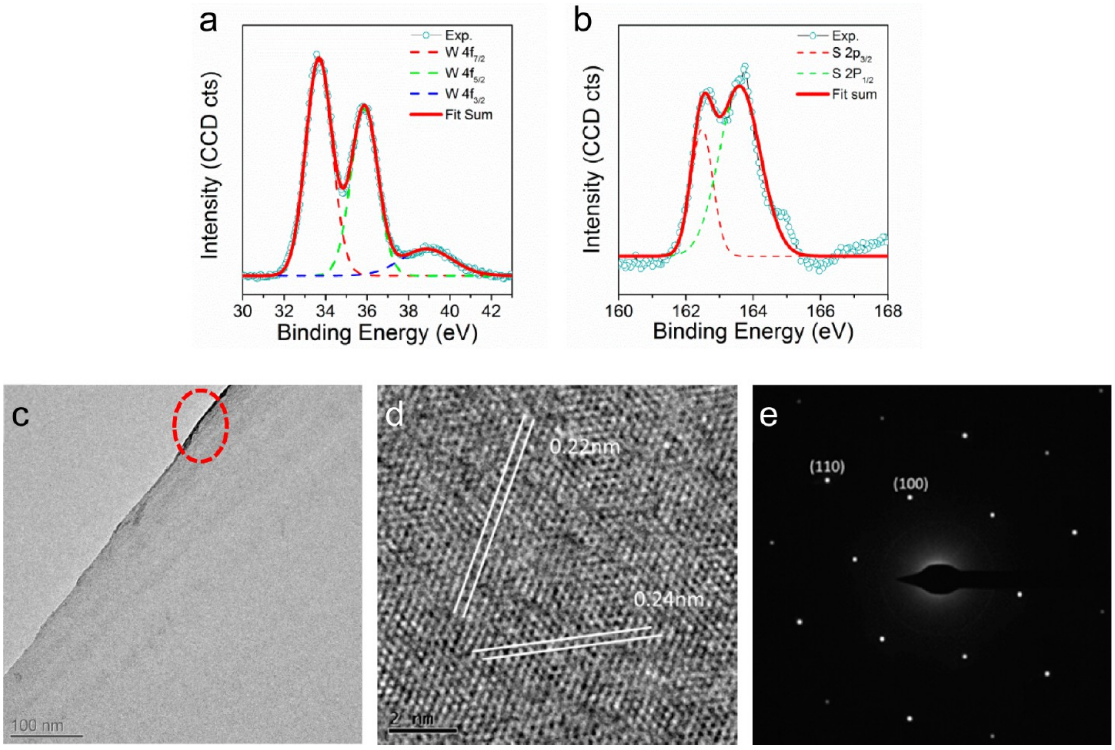

Figure 2. (a and b) XPS spectra of W 4f (a) and S 2p (b) for CVD WS_2. The three peaks at 33.67, 35.86, and 38.87 eV are attributed to the W $4f_{7/2}$, W $4f_{5/2}$, and W $4f_{3/2}$, respectively. The binding energy at 162.48 and 163.60 eV can be assigned to the S $2p_{1/2}$ and S $2p_{3/2}$, respectively. (c) Low-magnification TEM image of the WS_2 flake. The marked region shows the folded monolayer. The area at the edge clearly shows that the flake is monolayer. Scale bar: 100 nm. (d) High-resolution TEM image, the lattice spacings of 0.22 and 0.24 nm corresponding to the (100) and (110) planes are indicated. Scale bar: 2 nm. (e) Selected area diffraction pattern for monolayer WS_2, in which the diffraction spots (110) and (100) are assigned.

such as Al, S, O, C and W, can be resolved. Transmission electron microscopy (TEM) was also used to evaluate their microstructure and crystallinity. The low-magnification TEM image in Figure 2c shows the corner of monolayer WS_2 triangle where the contrast is relatively uniform with a folded region (marked red). Figure 2d shows the high-resolution TEM (HRTEM) image which clearly resolves the atomic lattice of WS_2. The selected area diffraction pattern (SEAD) is depicted in Figure 2e, in which the occurrence of only one set of hexagonal diffraction spots suggests that the WS_2 is single crystal over an aperture with a diameter of 100 μm.

To realize optoelectronic device applications, it is important to transfer the synthesized TMDs flakes from sapphire onto target substrates, such as silica, quartz and plastics. It is quite challenging to avoid damage to atomically thin samples as well as the growth substrate and also to maintain good continuity along with the original morphology. Here we demonstrate a PS mediated transfer process which relies on the capillary force at the air/water interface to delaminate WS_2 from the sapphire substrate, as schematically illustrated in Figure 3a. With the adaptation of methods developed to transfer graphene,[37] the modified transfer process of TMDs has four steps, *i.e.*, spin-coating PS on WS_2, etching in hot base, delaminating the polymer film from sapphire substrate in water, and fishing the materials onto target substrates. Previously, highly concentrated acid (HF) or base solution (*e.g.*, KOH, NaOH) was used to deep-etch the growth substrates (sapphire or SiO_2/Si) at high temperature (typical 80−100 °C) for 30−60 min so as to release the TMDs covered by polymer (usually poly(methyl methacrylate) (PMMA)).[20,25,27] In our experiment, the hydrophobic PS film can be detached from sapphire in water (see Figure S6) within 30 s after pre-etching in NaOH solution for 5 min, and films with 10 min pre-etching will release immediately from the growth substrate. However, long duration etching is found to cause severe damage to the surface of sapphire substrates (Figure S7d,e). Here, precise control of the temperature of NaOH solution below boiling point avoids the bubble generation and associated nonrecoverable damage to sapphire substrate and WS_2 samples (see Figure S7 b,d). It is assumed that the pre-etching for a short time (5−10 min) only opens small gaps between PS and sapphire at the sample edge, eliminating the need for exposure of the center of the sapphire substrate to the harsh etchant.

Besides the advantage of high efficiency, this new transfer technique offers good continuity and high quality WS_2 samples. To achieve nondestructive transfer of atomically thin layered materials, the key issue is

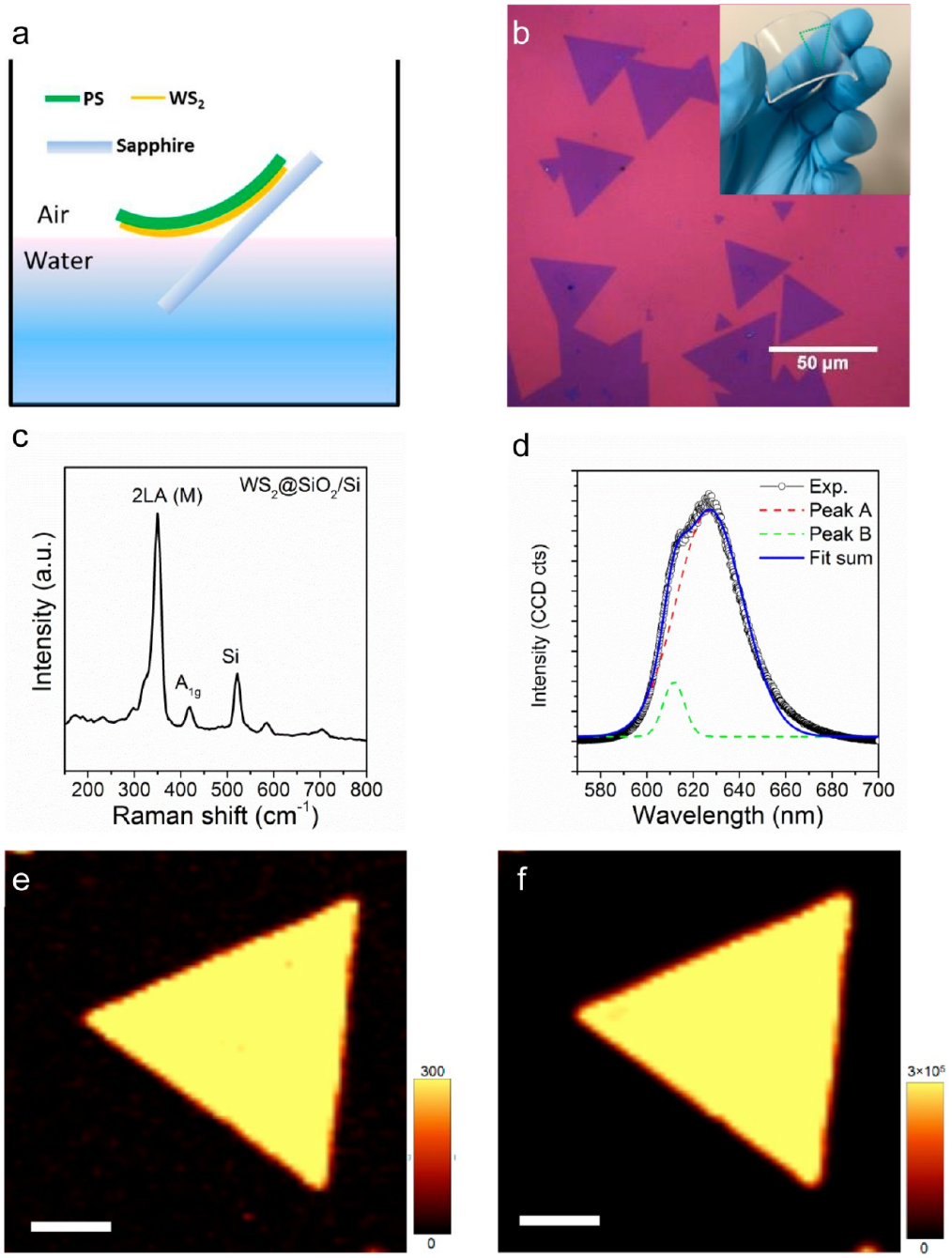

Figure 3. (a) Schematic image of the capillary force assisted delamination process. (b) Optical microscopy image of WS_2 flakes transferred on SiO_2/Si. Inset: A photograph of WS_2 monolayers transferred onto polydimethylsiloxane (PDMS). The sample is marked with a green triangle. (c) Raman spectrum of monolayer WS_2 after being transferred onto SiO_2/Si. (d) PL spectrum of monolayer WS_2 transferred onto SiO_2/Si substrate. Two subpeaks at 611 and 627 nm can be resolved with multipeak Lorentzian fitting. (e and f) Raman (e) and PL intensity (f) images of a typical WS_2 flake on SiO_2/Si by integration of Raman shift from 280 to 400 cm^{-1} and PL emission from 600 to 660 nm, respectively. Scale bar: 5 μm.

to avoid the residual stress by choosing suitable thickness of protecting material[37] and using a gentle, controllable and efficient delamination process as the transfer is actually a nonequilibrium process. Previously, a surface energy assisted transfer technique was demonstrated by using thick PS film to delaminate MoS_2 thin films from sapphire substrate.[38] The delamination by water drop is a self-happened process relying on the capillary force between hydrophobic PS and hydrophilic substrate. It should be noted that lots of broken pieces were observed while applying this method for transferring single crystals of monolayer MoS_2 due to the residual stress in thick PS film. To this point, we produced very thin PS film with a thickness of 100 nm as supporting layer for delamination. Rather than an uncontrollable process as described in ref 38, the delamination process is manually controlled by slowly feeding the sample into water with an

optimized delamination rate of ~0.3 cm^2/s in which the damage stress is minimized. As a result, the transferred monolayer crystals of WS_2 remain intact. Moreover, the transfer media PS has good solubility in toluene and can be completely removed in a few minutes on the spinner.[37] In contrast, the use of PMMA for transfer always leaves residues which significantly affect the electronic properties (see Figure S7).[37]

Figure 3b–d shows the optical microscopy image, Raman spectrum and PL spectrum of transferred monolayer WS_2 flakes on SiO_2/Si. We can see that the shape of the flakes transferred to SiO_2/Si was well preserved, and the contrast from the each flake was uniform, indicating that the transferred flakes are intact and clean (Figure 3a) and no residual particles were observed. The two characteristic Raman peaks of WS_2 are clearly resolved without shift after the transfer. Under the same excitation condition, the PL signal from WS_2 monolayer transferred onto SiO_2/Si substrate is about eight times that of the WS_2 monolayer grown directly on SiO_2/Si substrate (see Figure S8). The PL enhancement is attributed to the interference effect from SiO_2/Si substrate[27] and the doping effect induced by intercalated water beneath WS_2.[39−44] According to multipeak Lorentzian fitting, the PL spectrum of transferred WS_2 monolayer (shown in Figure 3d) comprises two subpeaks located at 611 and 627 nm. Figure 3e,f shows the images of Raman and PL intensity of transferred WS_2 monolayer. The relatively uniform intensity over the whole piece WS_2 suggests that the sample maintains good uniformity and continuity after transfer process.

The significant benefit of the new transfer technique is the recyclable use of sapphire substrates due to the minimal damage during transfer. We have demonstrated three successive growth-delamination-transfer cycles on the same sapphire substrate and monitored the quality of three batches of WS_2 monolayers. Figure 4a–c shows the optical images of three different batches of samples, *i.e.*, the first cycle (W1), the second cycle (W2), and the third cycle (W3). It was found that the shape of all crystals were well retained, in which the overall reflectance contrast was uniform under the same illumination. More than 95% of the crystals were monolayer WS_2, though occasionally we could also observe some additional layers growth (the small bright spots in Figure 4a–c). The Raman images in Figure 4d–f show that the WS_2 monolayers from each cycle are elementally uniform. The Raman spectra in Figure 4j also reveal that the three batches of samples have similar characteristic peaks without peak shift. On the basis of the micro-Raman spectroscopy, there is no peak shift within one piece of WS_2 from the center to the edge (see Figure S9a). However, the PL images (Figure 4g–i) of as-grown WS_2 monolayers on sapphire showed interesting light emission properties which was never reported on WS_2 before. First, the PL intensity at the center is 10 times higher than that at the edge. And the peak position experiences a small blue-shift (2 nm) from the center to the edge (Figure S9b). It is proposed that the edge was grown during the cooling stage and the relatively lower PL emission is correlated to the sulfur deficiency.[31,45] Second, the PL emission in W1 sample shows periodic enhancement at the central area with an intensity peak-to-peak distance of ~250 nm. The distance is nearly the same as the period of atomic terrace on sapphire substrate which will be discussed later. Lastly, the PL emission from three batches of samples increases as the substrate recycles, *i.e.*, the PL intensity from W3 was nearly 10 times as high as W1 while the peak red-shifts from 620 to 630 nm, as shown in Figure 4k. It is suggested that the water intercalated in the atomic steps of the recycled sapphire surface is the main reason for the PL enhancement as it causes *p*-type doping to our monolayer WS_2 flakes.[13,40−42,50]

To understand the origin of the evolution in the PL image at the sample center, AFM was performed on sapphire substrates with increasing cycles (S1, S2, and S3) and the monolayer WS_2 grown atop. Figure 5a–c shows the topography of S1–3 sapphire substrates. The atomically flat terrace of sapphire can be well resolved and the step is ~0.2 nm. The recycled substrates show the similar morphology to S1 and the presence of well-ordered atomic steps on the recycled substrates manifest that the surface is good with perfect atomically flat terraces. The root-mean-square (rms) roughness of fresh and reused sapphire substrates was measured to be 0.180 nm (S1), 0.161 nm (S2), and 0.155 nm (S3). The tiny difference in the surface roughness verified minor damage to sapphire substrate during pre-etching in base solution. As we expected, the morphology of grown WS_2 monolayer follows that of sapphire surface very well, as shown in Figure 5d–f. In particular, we found that distinct contrast difference between the center and edge of WS_2 triangle crystal. As the crystal grows, it expands from one terrace to the next one, and the step edges bend toward the uphill direction as one goes from the edge to the center region, which makes the center of the crystal a little bit thicker. In addition, we are also able to observe the atomic scale terrace within the WS_2 flake as the crystal follows the feature of the substrate seamlessly. The possible strain at the terrace as well as postgrowth hydroxylation and hydration[50] are responsible for periodic PL emission observed in Figure 4g,h. In the third cycle, the terraces on sapphire or within WS_2 crystal are relatively blurred. As a result, the PL emission (Figure 4i) does not show periodical strips.

We further fabricate field-effect transistors to evaluate the electronic properties of WS_2 monolayers

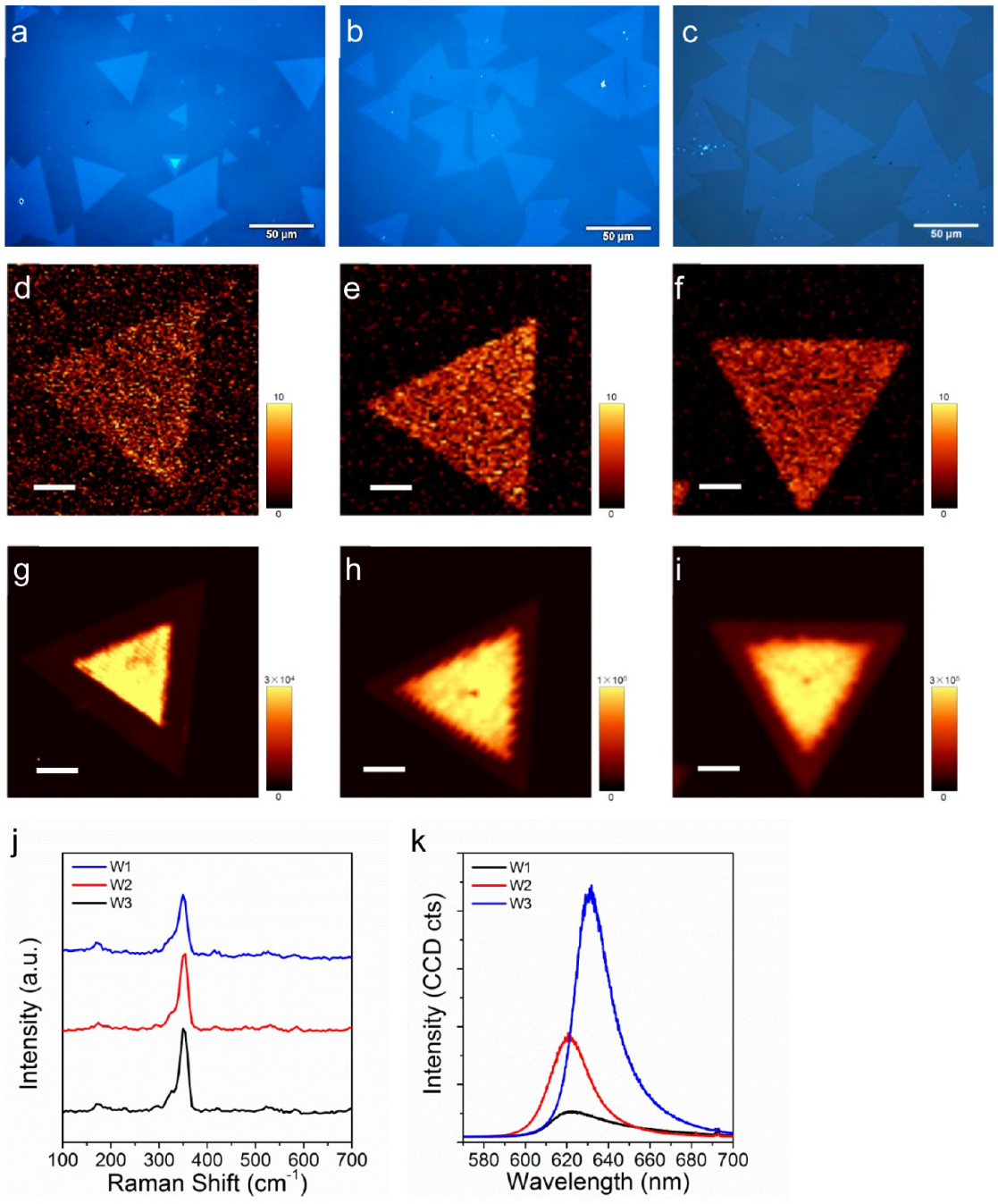

Figure 4. (a–c) Optical microscopy images of WS_2 monolayer triangular flakes grown on S1, S2, and S3 sapphire substrates. (d–f) Raman intensity images of W1, W2, and W3 samples on sapphire by integration from 280 to 400 cm^{-1}. Scale bar: 4 μm. (g–i) PL intensity images of W1, W2, and W3 samples on sapphire by integration from 590 to 690 nm. Scale bar: 4 μm. (j and k) Raman and PL spectra obtained from the center of W1, W2, and W3.

grown on recycled sapphire substrate. To make the transistor device, WS_2 monolayers are delaminated and transferred onto SiO_2/Si substrates using the technique discussed above. Figure 5i schematically illustrates the configuration of the transistor device with a back gate. The typical transfer curve (Figure 5j) of WS_2 transistor device reveals that the as-transferred WS_2 is *n*-type semiconducting material with an ON/OFF ratio up to 10^5. The neutral point of the transfer curve is nearly at zero gate voltage, which further indicates complete removal of polymer coating layer and a low intrinsic doping level in the transferred WS_2 monolayers.[8,27] The field-effect mobility of the device was extracted by

$$\mu = \frac{dI_d}{dV_g}\frac{L}{W}\frac{1}{C_i}\frac{1}{V_d} \quad (2)$$

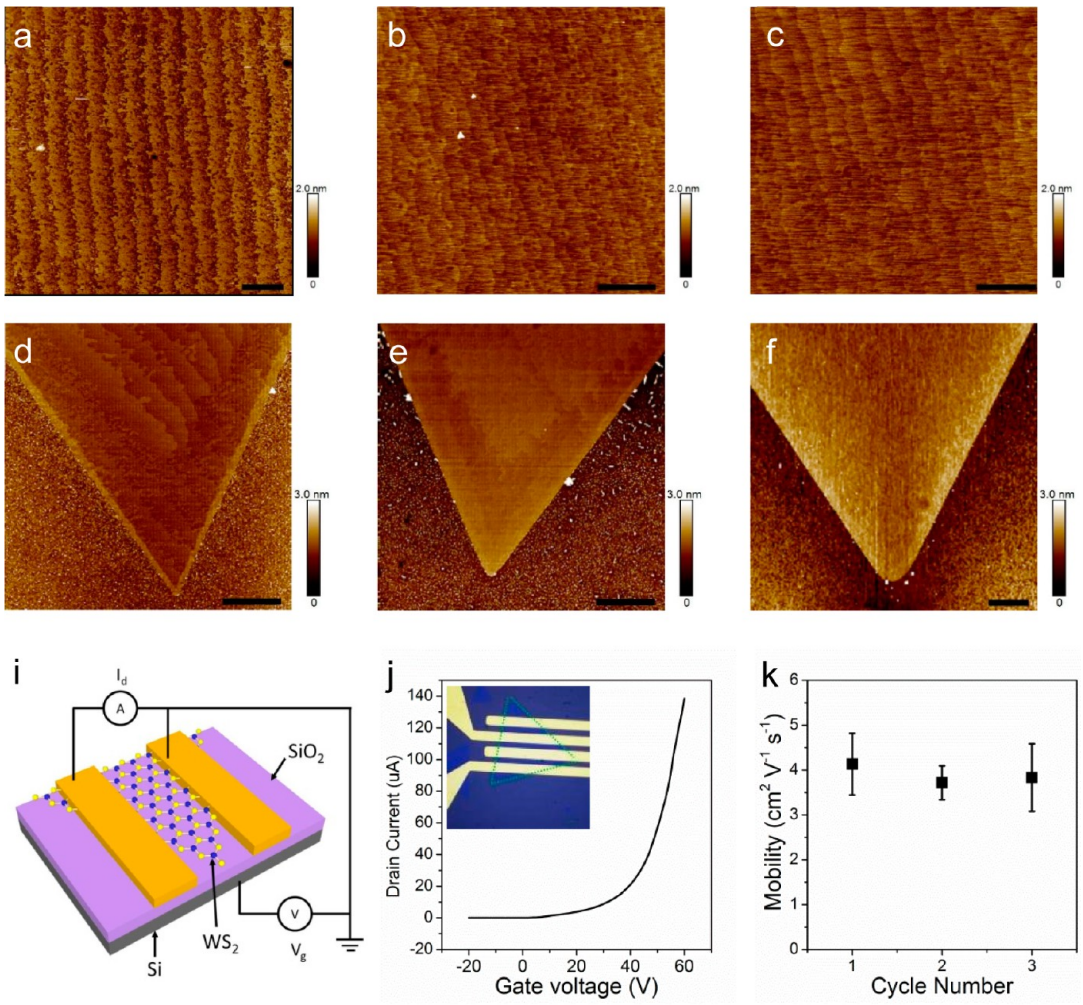

Figure 5. (a−c) AFM topography images of S1, S2, and S3 sapphire substrates. Scale bar: 400 nm. (d−f) AFM height images of W1, W2, and W3. Scale bar: 1 μm. (i) Schematic image of a WS_2 FET device. (j) The I_d *vs* V_g curve of WS_2 transistor device measured in ambient condition. Inset: optical microscopy image of a WS_2 FET device. Scale bar: 10 μm. (k) Electron mobility as a function of the cycle number.

where I_d is the drain current, V_g is the gate voltage, dI_d/dV_g is the slope, L and W are the channel length and channel width, respectively. The capacitance C_i between the channel and the back gate per unit area is estimated to be ~1.2 F cm^{-2} ($C_i = \varepsilon_0\varepsilon_r/d$, where ε_0 is the permittivity of free space, $\varepsilon_r = 3.9$ and $d = 285$ nm).[46] It is concluded that WS_2 monolayers transferred from fresh sapphire substrate have an average electron mobility of 4.1 $cm^2 V^{-1} s^{-1}$, which is much higher than that of WS_2 monolayer grown by conventional CVD and atomic layer deposition (ALD).[28,27] As reported previously, high-k dielectric gate insulators can further improve the mobility by screening the phonon scattering.[6,28] In this case, no such technique was applied, and we believe that higher mobility can be achieved by introducing high-k dielectric gate and optimization of the electrodes contact.[47−49] Furthermore, WS_2 monolayers grown in subsequent cycles have comparable electron mobility, *i.e.*, 3.7 $cm^2 V^{-1} s^{-1}$ for W2 and 3.8 $cm^2 V^{-1} s^{-1}$ for W3.

CONCLUSIONS

Large area (domain size of more than 100 μm), triangular monolayer WS_2 crystals were grown on sapphire substrates using APCVD which has no ventilation system. Compared with WS_2 crystals grown on SiO_2/Si substrates using the same method, the monolayer WS_2 crystals grown on sapphire has better quality in terms of stronger and narrower PL emission. A polystyrene (PS) mediated delamination process was used to transfer WS_2 flakes onto arbitrary substrates with excellent continuity. Due to the hydrophobicity of PS and the capillary force at air/water interface, WS_2 flakes can be effectively peeled off from sapphire substrate, which greatly reduces the etching time in base solution and in turn causes minor damage to the sapphire substrate. The gentle and nondestructive transfer technique affords the possibility for recyclable use of costly sapphire crystals. We have also demonstrated that the transferred WS_2 flakes exhibited

comparable electron mobility after several growth cycles on the reused sapphire substrate. In conclusion, the growth and transfer techniques described here could greatly improve the efficiency and reduce the production cost, and are transplantable to other atomically thin TMD materials.

METHODS

WS_2 Growth. The growth of WS_2 was performed in a quartz tube with the diameter of 2 in. A 250 sccm ultrahigh purity argon at atmospheric pressure was flowing as carrier gas. In a typical experiment, WO_3 (50 mg, Sigma-Aldrich 204781) and sapphire substrate (8 mm × 8 mm) were placed at the center and downstream of the furnace (18 cm from the center), respectively. The sulfur powder (500 mg, Sigma-Aldrich, 213292) was loaded upstream and heated independently. The furnace and the sulfur are heated to 900 and 180 °C within 30 min and kept for 60 min, respectively. The furnace was then cooled naturally with the cover open. H_2 with the flow rate of 5 sccm was introduced into the quartz chamber once the temperature reached 900 °C. To recycle the sapphire substrates, they were cleaned with a solution mixture of $NH_3/H_2O_2/H_2O$ (1:1:5, v/v) before growth. The second and third growth cycles of WS_2 were performed on the same sapphire substrate with the same synthesis condition.

Transfer. PS was used as the supporting film to peel off the WS_2 crystals from sapphire substrates. PS (M_w ~192 000) dispersed in toluene solution (50 mg/mL) was spin-coated on top of the sample at a speed of 3000 rpm. The resulting thickness of PS film calibrated with ellipsometery spectroscopy was ~100 nm. The edge of the PS film was scribed with scalpel to lead in etching solution. Then, the samples were pre-etched in hot NaOH solution (2 mol/L, 90 °C) for 10 min followed with delamination in water for a few seconds. Lastly, the samples were rinsed with deionized-water thrice before fishing up onto target substrates. The PS coating was removed with toluene after baking the sample at 120 °C for 30 min. The TEM samples were prepared with the same method.

Characterizations. Raman and PL measurements were performed using confocal microscope system (WITec, alpha 300R) with a 100× objective (NA = 0.9) in an ambient condition. A 532 nm laser was used to excite samples which were placed on a piezo crystal-controlled scanning stage. The spectra are collected using 600 line/mm grating. To avoid the sample damage, low laser power (50 μW) is applied during the measurements. The topography and thickness of WS_2 samples were characterized by AFM (Bruker, Dimension Icon SPM) with tapping mode. XPS was conducted in an ultrahigh vacuum photoemission spectroscopy system (Kratos, AXIS Ultra-DLD) with the chamber pressure less than 5×10^{-10} Torr.

Device Fabrications. The field-effect transistor devices were fabricated on WS_2 monolayers that had been transferred onto SiO_2/Si. The electrodes were patterned with standard UV-light direct write lithography followed by electron-beam deposition of Ti/Au (5/50 nm) in vacuum with a chamber pressure $<6 \times 10^{-6}$ Torr. The channel length between the source and drain electrodes was around 5 μm. The devices were annealed at 200 °C for 2 h in argon atmosphere prior to testing. The drain current I_d as a function of bias voltage V and gate voltage V_g was investigated using two-channel source meter unit (Agilent, B2902A) in ambient condition.

Conflict of Interest: The authors declare no competing financial interest.

Acknowledgment. This work was supported by ARC DECRA (DE120101569) and DSI top-up grant, DP (DP140101501), Engineering Seed Fund in Monash University. Z. Xu acknowledges support from the APA and IPRS scholarship. Q. Bao also acknowledges the support from 863 Program (Grant No. 2013AA031903), the youth 973 program (2015CB932700), the National Natural Science Foundation of China (Grant No. 51222208, 51290273, 91433107). This work was performed in part at the Melbourne Centre for Nanofabrication (MCN) in the Victorian Node of the Australian National Fabrication Facility (ANFF). Z. Xu acknowledges Dr. Yunzhou Xue for fruitful discussions.

Supporting Information Available: Additional photographs and optical images, Raman, PL, XPS and TEM characterization results. The Supporting Information is available free of charge on the ACS Publications website at DOI: 10.1021/acsnano.5b01480.

REFERENCES AND NOTES

1. Lopez-Sanchez, O.; Alarcon Llado, E.; Koman, V.; Fontcuberta i Morral, A.; Radenovic, A.; Kis, A. Light Generation and Harvesting in a Van Der Waals Heterostructure. *ACS Nano* **2014**, *8*, 3042–3048.
2. Pospischil, A.; Mueller, T. Solar-Energy Conversion and Light Emission in an Atomic Monolayer *p*–*n* Diode. *Nat. Nanotechnol.* **2014**, *9*, 257–262.
3. Ross, J. S.; Klement, P.; Jones, A. M.; Ghimire, N. J.; Yan, J.; Mandrus, D. G.; Taniguchi, T.; Watanabe, K.; Kitamura, K.; Yao; et al. Electrically Tunable Excitonic Light-Emitting Diodes Based on Monolayer WSe_2 *p-n* Junctions. *Nat. Nanotechnol.* **2014**, *9*, 268–272.
4. Zhang, Y. J.; Oka, T.; Suzuki, R.; Ye, J. T.; Iwasa, Y. Electrically Switchable Chiral Light-Emitting Transistor. *Science* **2014**, *344*, 725–728.
5. Lopez-Sanchez, O.; Lembke, D.; Kayci, M.; Radenovic, A.; Kis, A. Ultrasensitive Photodetectors Based on Monolayer MoS_2. *Nat. Nanotechnol.* **2013**, *8*, 497–501.
6. Radisavljevic, B.; Radenovic, A.; Brivio, J.; Giacometti, V.; Kis, A. Single-Layer MoS_2 Transistors. *Nat. Nanotechnol.* **2011**, *6*, 147–150.
7. Pu, J.; Yomogida, Y.; Liu, K. K.; Li, L. J.; Iwasa, Y.; Takenobu, T. Highly Flexible MoS_2 Thin-Film Transistors with Ion Gel Dielectrics. *Nano Lett.* **2012**, *12*, 4013–4017.
8. Ovchinnikov, D.; Allain, A.; Huang, Y. S.; Dumcenco, D.; Kis, A. Electrical Transport Properties of Single-Layer WS_2. *ACS Nano* **2014**, *8*, 8174–8181.
9. Allain, A.; Kis, A. Electron and Hole Mobilities in Single-Layer WSe_2. *ACS Nano* **2014**, *8*, 7180–7185.
10. Zhang, Y.; Chang, T. R.; Zhou, B.; Cui, Y. T.; Yan, H.; Liu, Z.; Schmitt, F.; Lee, J.; Moore, R.; Chen, Y.; et al. Direct Observation of the Transition from Indirect to Direct Bandgap in Atomically Thin Epitaxial $MoSe_2$. *Nat. Nanotechnol.* **2014**, *9*, 111–115.
11. Mak, K. F.; Lee, C.; Hone, J.; Shan, J.; Heinz, T. F. Atomically Thin MoS_2: A New Direct-Gap Semiconductor. *Phys. Rev. Lett.* **2010**, *105*, 136805.
12. Splendiani, A.; Sun, L.; Zhang, Y.; Li, T.; Kim, J.; Chim, C. Y.; Galli, G.; Wang, F. Emerging Photoluminescence in Monolayer MoS_2. *Nano Lett.* **2010**, *10*, 1271–1275.
13. Zhao, W.; Ghorannevis, Z.; Chu, L.; Toh, M.; Kloc, C.; Tan, P. H.; Eda, G. Evolution of Electronic Structure in Atomically Thin Sheets of WS_2 and WSe_2. *ACS Nano* **2013**, *7*, 791–797.
14. Mak, K. F.; He, K.; Lee, C.; Lee, G. H.; Hone, J.; Heinz, T. F.; Shan, J. Tightly Bound Trions in Monolayer MoS_2. *Nat. Mater.* **2013**, *12*, 207–211.
15. Liu, Y.; Nan, H.; Wu, X.; Pan, W.; Wang, W.; Bai, J.; Zhao, W.; Sun, L.; Wang, X.; Ni, Z. Layer-by-Layer Thinning of MoS_2 by Plasma. *ACS Nano* **2013**, *7*, 4202–4209.
16. Yu, Y.; Li, C.; Liu, Y.; Su, L.; Zhang, Y.; Cao, L. Controlled Scalable Synthesis of Uniform, High-Quality Monolayer and Few-Layer MoS_2 Films. *Sci. Rep.* **2013**, *3*, 1866.
17. Ling, X.; Lee, Y. H.; Lin, Y.; Fang, W.; Yu, L.; Dresselhaus, M. S.; Kong, J. Role of the Seeding Promoter in MoS_2 Growth by Chemical Vapor Deposition. *Nano Lett.* **2014**, *14*, 464–472.

18. Shi, Y.; Zhou, W.; Lu, A. Y.; Fang, W.; Lee, Y. H.; Hsu, A. L.; Kim, S. M.; Kim, K. K.; Yang, H. Y.; Li, L. J.; et al. Van Der Waals Epitaxy of MoS_2 Layers Using Graphene as Growth Templates. *Nano Lett.* **2012**, *12*, 2784–2791.
19. Huang, Y.; Wu, J.; Xu, X.; Ho, Y.; Ni, G.; Zou, Q.; Koon, G. K. W.; Zhao, W.; Castro Neto, A. H.; Eda, G.; et al. An Innovative Way of Etching MoS_2: Characterization and Mechanistic Investigation. *Nano Res.* **2013**, *6*, 200–207.
20. Lin, Y. C.; Zhang, W.; Huang, J. K.; Liu, K. K.; Lee, Y. H.; Liang, C. T.; Chu, C. W.; Li, L. J. Wafer-Scale MoS_2 Thin Layers Prepared by MoO_3 Sulfurization. *Nanoscale* **2012**, *4*, 6637–6641.
21. Tan, L. K.; Liu, B.; Teng, J. H.; Guo, S.; Low, H. Y.; Loh, K. P. Atomic Layer Deposition of a MoS_2 Film. *Nanoscale* **2014**, *6*, 10584–10588.
22. Cheng, Y.; Yao, K.; Yang, Y.; Li, L.; Yao, Y.; Wang, Q.; Zhang, X.; Han, Y.; Schwingenschlögl, U. Van Der Waals Epitaxial Growth of MoS_2 on SiO_2/Si by Chemical Vapor Deposition. *RSC Adv.* **2013**, *3*, 17287.
23. Wu, J.; Li, H.; Yin, Z.; Li, H.; Liu, J.; Cao, X.; Zhang, Q.; Zhang, H. Layer Thinning and Etching of Mechanically Exfoliated MoS_2 Nanosheets by Thermal Annealing in Air. *Small* **2013**, *9*, 3314–3319.
24. Zhan, Y.; Liu, Z.; Najmaei, S.; Ajayan, P. M.; Lou, J. Large-Area Vapor-Phase Growth and Characterization of MoS_2 Atomic Layers on a SiO_2 Substrate. *Small* **2012**, *8*, 966–971.
25. Elias, A. L.; Perea-Lopez, N.; Castro-Beltran, A.; Berkdemir, A.; Lv, R.; Feng, S.; Long, A. D.; Hayashi, T.; Kim, Y. A.; Endo, M.; Gutierrez, H. R.; et al. Controlled Synthesis and Transfer of Large-Area WS_2 Sheets: From Single Layer to Few Layers. *ACS Nano* **2013**, *7*, 5235–5242.
26. Okada, M.; Sawazaki, T.; Watanabe, K.; Taniguch, T.; Hibino, H.; Shinohara, H.; Kitaura, R. Direct Chemical Vapor Deposition Growth of WS_2 Atomic Layers on Hexagonal Boron Nitride. *ACS Nano* **2014**, *8*, 8273–8277.
27. Zhang, Y.; Zhang, Y.; Ji, Q.; Ju, J.; Yuan, H.; Shi, J.; Gao, T.; Ma, D.; Liu, M.; Chen, Y.; et al. Controlled Growth of High-Quality Monolayer WS_2 Layers on Sapphire and Imaging Its Grain Boundary. *ACS Nano* **2013**, *7*, 8963–8971.
28. Song, J. G.; Park, J.; Lee, W.; Choi, T.; Jung, H.; Lee, C. W.; Hwang, S. H.; Myoung, J. M.; Jung, J. H.; et al. Layer-Controlled, Wafer-Scale, and Conformal Synthesis of Tungsten Disulfide Nanosheets Using Atomic Layer Deposition. *ACS Nano* **2013**, *7*, 11333–11340.
29. Cong, C.; Shang, J.; Wu, X.; Cao, B.; Peimyoo, N.; Qiu, C.; Sun, L.; Yu, T. Synthesis and Optical Properties of Large-Area Single-Crystalline 2d Semiconductor WS_2 monolayer from Chemical Vapor Deposition. *Adv. Opt. Mater.* **2014**, *2*, 131–136.
30. Li, H.; Zhang, Q.; Yap, C. C. R.; Tay, B. K.; Edwin, T. H. T.; Olivier, A.; Baillargeat, D. From Bulk to Monolayer MoS_2: Evolution of Raman Scattering. *Adv. Funct. Mater.* **2012**, *22*, 1385–1390.
31. Peimyoo, N.; Shang, J.; Cong, C.; Shen, X.; Wu, X.; Yeow, E. K.; Yu, T. Nonblinking, Intense Two-Dimensional Light Emitter: Monolayer WS_2 Triangles. *ACS Nano* **2013**, *7*, 10985–10994.
32. Gutierrez, H. R.; Perea-Lopez, N.; Elias, A. L.; Berkdemir, A.; Wang, B.; Lv, R.; Lopez-Urias, F.; Crespi, V. H.; Terrones, H.; Terrones, M. Extraordinary Room-Temperature Photoluminescence in Triangular WS_2 Monolayers. *Nano Lett.* **2013**, *13*, 3447–3454.
33. Rong, Y.; Fan, Y.; Leen Koh, A.; Robertson, A. W.; He, K.; Wang, S.; Tan, H.; Sinclair, R.; Warner, J. H. Controlling Sulphur Precursor Addition for Large Single Crystal Domains of WS_2. *Nanoscale* **2014**, *6*, 12096–12103.
34. Berkdemir, A.; Gutiérrez, H. R.; Botello-Méndez, A. R.; Perea-López, N.; Elías, A. L.; Chia, C.-I.; Wang, B.; Crespi, V. H.; López-Urías, F.; Charlier, J.-C.; Terrones, H.; et al. Identification of Individual and Few Layers of WS_2 Using Raman Spectroscopy. *Sci. Rep.* **2013**, *3*.
35. Sercombe, D.; Schwarz, S.; Del Pozo-Zamudio, O.; Liu, F.; Robinson, B. J.; Chekhovich, E. A.; Tartakovskii, I. I.; Kolosov, O.; Tartakovskii, A. I. Optical Investigation of the Natural Electron Doping in Thin MoS_2 Films Deposited on Dielectric Substrates. *Sci. Rep.* **2013**, *3*, 3489.
36. Shpak, A. P.; Korduban, A. M.; Kulikov, L. M.; Kryshchuk, T. V.; Konig, N. B.; Kandyba, V. O. XPS Studies of the Surface of Nanocrystalline Tungsten Disulfide. *J. Electron Spectrosc. Relat. Phenom.* **2010**, *181*, 234–238.
37. Song, J.; Kam, F. Y.; Png, R. Q.; Seah, W. L.; Zhuo, J. M.; Lim, G. K.; Ho, P. K.; Chua, L. L. A General Method for Transferring Graphene onto Soft Surfaces. *Nat. Nanotechnol.* **2013**, *8*, 356–362.
38. Gurarslan, A.; Yu, Y.; Su, L.; Yu, Y.; Suarez, F.; Yao, S.; Zhu, Y.; Ozturk, M.; Zhang, Y.; Cao, L. Surface-Energy-Assisted Perfect Transfer of Centimeter-Scale Mono Layer and Few-Layer MoS_2 Films onto Arbitrary Substrates. *ACS Nano* **2014**, *8*, 11522–11528.
39. Tongay, S.; Zhou, J.; Ataca, C.; Liu, J.; Kang, J. S.; Matthews, T. S.; You, L.; Li, J.; Grossman, J. C.; Wu, J. Broad-Range Modulation of Light Emission in Two-Dimensional Semiconductors by Molecular Physisorption Gating. *Nano Lett.* **2013**, *13*, 2831–2836.
40. Peimyoo, N.; Yang, W.; Shang, J.; Shen, X.; Wang, Y.; Yu, T. Chemically Driven Tunable Light Emission of Charged and Neutral Excitons in Monolayer WS_2. *ACS Nano* **2014**, *8*, 11320–11329.
41. Mouri, S.; Miyauchi, Y.; Matsuda, K. Tunable Photoluminescence of Monolayer MoS_2 *via* Chemical Doping. *Nano Lett.* **2013**, *13*, 5944–5948.
42. Yang, L.; Majumdar, K.; Liu, H.; Du, Y.; Wu, H.; Hatzistergos, M.; Hung, P. Y.; Tieckelmann, R.; Tsai, W.; Hobbs, C.; et al. Chloride Molecular Doping Technique on 2D Materials: WS_2 and MoS_2. *Nano Lett.* **2014**, *14*, 6275–6280.
43. Mitioglu, A.; Plochocka, P.; Jadczak, J.; Escoffier, W.; Rikken, G.; Kulyuk, L.; Maude, D. Optical Manipulation of the Exciton Charge State in Single-Layer Tungsten Disulfide. *Phys. Lett. B* **2013**, *88*, No. 245403 .
44. Newaz, A. K. M.; Prasai, D.; Ziegler, J. I.; Caudel, D.; Robinson, S.; Haglund, R. F., Jr; Bolotin, K. I. Electrical Control of Optical Properties of Monolayer MoS_2. *Solid State Commun.* **2013**, *155*, 49–52.
45. Wang, X.; Gong, Y.; Shi, G.; Chow, W. L.; Keyshar, K.; Ye, G.; Vajtai, R.; Lou, J.; Liu, Z.; Ringe, E.; et al. Chemical Vapor Deposition Growth of Crystalline Monolayer $MoSe_2$. *ACS Nano* **2014**, *8*, 5125–5131.
46. Najmaei, S.; Liu, Z.; Zhou, W.; Zou, X.; Shi, G.; Lei, S.; Yakobson, B. I.; Idrobo, J. C.; Ajayan, P. M.; Lou, J. Vapour Phase Growth and Grain Boundary Structure of Molybdenum Disulphide Atomic Layers. *Nat. Mater.* **2013**, *12*, 754–759.
47. Liu, W.; Kang, J.; Sarkar, D.; Khatami, Y.; Jena, D.; Banerjee, K. Role of Metal Contacts in Designing High-Performance Monolayer *n*-Type WSe_2 Field Effect Transistors. *Nano Lett.* **2013**, *13*, 1983–1990.
48. Chuang, H. J.; Tan, X.; Ghimire, N. J.; Perera, M. M.; Chamlagain, B.; Cheng, M. M.; Yan, J.; Mandrus, D.; Tomanek, D.; Zhou, Z. High Mobility WSe_2 *p*- and *n*-Type Field-Effect Transistors Contacted by Highly Doped Graphene for Low-Resistance Contacts. *Nano Lett.* **2014**, *14*, 3594–3601.
49. Fang, H.; Chuang, S.; Chang, T. C.; Takei, K.; Takahashi, T.; Javey, A. High-Performance Single Layered WSe_2 *p*-FETs with Chemically Doped Contacts. *Nano Lett.* **2012**, *12*, 3788–3792.
50. Zheng, C.; Xu, Z.-Q.; Zhang, Q.; Edmonds, M. T.; Watanabe, K.; Taniguchi, T.; Bao, Q.; Fuhrer, M. S. Profound Effect of Substrate Hydroxylation and Hydration on Electronic and Optical Properties of Monolayer MoS_2. *Nano Lett.* **2015**, *15*, 3096−3102.